Fluid–Structure Interaction Simulation of an Emergency Recovery Parachute for a Flying Car

Koki Fukusumi[1[0009-0002-9907-2954]], Ayato Takii[2[0000-0003-3257-7640]], Masashi Yamakawa[1, 3, 4[0000-0001-5960-2602]], Yusei Kobayashi[1, 4[0000-0002-5690-2033]], Takahiro Ikeda[3, 4[0009-0008-7496-9056]], Shinichi Asao[5[0000-0003-4326-8480]] and Seiichi Takeuchi[5]

[1] Kyoto Institute of Technology, Matsugasaki, Sakyo-ku, Kyoto 606-8585, Japan
m25623031@kit.edu.ac.jp
[2] Kobe University, Rokkodai, 1-1 Rokkodai-cho, Nada-ku, Kobe, Hyogo 657-8501, Japan
[3] Center for the Possible Futures, Kyoto Institute of Technology, Matsugasaki, Sakyo-ku, Kyoto 606-8585, Japan
[4] High-Performance Simulation Research Center, Kyoto Institute of Technology, Matsugasaki, Sakyo-ku, Kyoto 606-8585, Japan
[5] College of Industrial Technology, 1-27-1, Amagasaki, Hyogo 661-0047, Japan

Abstract. In recent years, emergency recovery parachutes have been considered as a passive safety measure for flying cars, which are regarded as a form of Urban Air Mobility, to mitigate damage to onboard passengers and people on the ground in the event of catastrophic failures such as electrical power loss. However, their design and verification remain challenging due to low-altitude deployment, potential interference between suspension lines and propellers, and the difficulty of conducting full-scale drop tests, which are costly and involve significant risk. Therefore, a numerical framework capable of reproducing the coupled behavior of a vehicle–parachute system is essential. In this study, a fluid–structure interaction simulation framework is applied, in which a moving-boundary fluid solver based on an unstructured moving-grid finite-volume method for solving the Euler equations is weakly coupled with a structural solver using Project Chrono. Numerical wind-tunnel and free-fall FSI simulations are conducted. The results show that gore reinforcement cables govern the inflated canopy shape and constitute a primary factor in determining the mean drag, with an approximately 19% difference in projected area observed between configurations. In addition, canopy elasticity induces unsteady drag fluctuations associated with periodic deformation, which are not captured by rigid models. In the free-fall simulation, the descent velocity decreases from 9.81 m/s to 8.53 m/s in approximately 1.43 s, approaching a quasi-steady descent state where drag balances the system weight. These findings highlight the importance of structural modeling in parachute design and provide fundamental insights for the safety design of flying cars.

Keywords: UAM, eVTOL, Emergency Recovery Parachute, FSI, Numerical Simulation

ICCS Camera Ready Version 2026
To cite this paper please use the final published version:
DOI: 10.1007/978-3-032-29921-5_7

1 Introduction

1.1 Parachute for a Flying Car

In recent years, flying car transportation systems that utilize near-ground space in urban areas have attracted growing attention, and major aerospace and automotive manufacturers worldwide have entered this field. A wide variety of takeoff/landing and cruise configurations have been proposed, and flying cars represent a next-generation mobility concept capable of exploiting near-ground space to provide high-speed, flexible transportation. To realize such systems, multifaceted research and development efforts are being conducted to address numerous technical, commercial, and ethical challenges [1, 2]. Among these issues, one of the most critical and challenging is safety. If a flying car were to crash from above an urban area, severe consequences are foreseeable for onboard passengers and for people and structures on the ground. Adverse weather conditions, failures of onboard components, and human error can cause route deviations and may lead to loss of control or collisions [3]. In particular, for multirotor and distributed electric propulsion configurations, where active stabilization is indispensable, the loss of electrical power can be catastrophic. Unlike helicopters and fixed-wing aircraft, such vehicles cannot rely on failure mitigation measures such as autorotation or gliding, and may therefore become uncontrollable following a loss of propulsion power [4].

For these reasons, several manufacturers are considering parachute recovery systems as an effective passive safety measure by substantially reducing the descent speed. ARIDGE has conducted full-scale tests in which a flying car was brought to the ground using a parachute, demonstrating its effectiveness [5]. In addition, as a parachute provider for light aircraft, BRS (Ballistic Recovery Systems) operates a ballistic recovery system business and has recorded numerous successful saves [6]. However, several challenges must be addressed to apply such ballistic recovery systems to flying cars. First, the relatively low cruising altitude may limit the time available for sufficient deceleration. Second, there is a risk that the parachute suspension lines may become entangled with the propellers [7, 8]. To maximize the performance of parachutes designed for flying cars, meticulous design and validation are indispensable. However, flying cars have various configurations, with differences in vehicle geometry and cruising speed; therefore, parachutes must be designed individually for each vehicle, which complicates the development process. To address these challenges, it is desirable to predict in advance the free-fall behavior of the coupled vehicle–parachute system. However, full-scale drop tests are costly and involve significant risk, making comprehensive validation at early design stages difficult. Therefore, it is essential to establish a numerical simulation framework capable of quantitatively evaluating the vehicle–parachute system while accounting for fluid forces and structural deformation.

1.2 FSI Simulation of a Parachute

Because a parachute undergoes large elastic deformation during both deployment and descent, a coupled simulation framework that integrates moving-boundary fluid

ICCS Camera Ready Version 2026
To cite this paper please use the final published version:
DOI: 10.1007/978-3-032-29921-5_7

simulation with structural simulation is required. Fluid–structure interaction (FSI) has been widely applied in various fields, including aerospace engineering, and numerous studies have investigated parachute systems. TAFSM (The Team for Advanced Flow Simulation and Modeling) has conducted parachute FSI research since 1997 and has developed multiple numerical approaches [9]. Although various coupled approaches and interface-capturing methods have been proposed for parachute modeling, few studies have focused on emergency parachutes for flying cars.

In simulation-based validation at the early stages of flying-car design, it is important to appropriately simplify the physical model while maintaining acceptable accuracy, thereby reducing computational cost and accelerating the design cycle. As a first step, this study applies an FSI model to an emergency parachute system for a flying car. Specifically, a computational framework is constructed by weakly coupling a moving-boundary fluid solver based on an unstructured moving-grid finite-volume method [10, 11] with the open-source structural simulation platform Project Chrono [12, 13]. In addition, numerical wind-tunnel FSI simulations of the parachute were conducted based on the simulation procedures and material properties reported in previous studies [14, 15]. The validity and necessity of modeling the parachute as an elastic body were examined through comparative simulations with a rigid-body model. Finally, a free-fall FSI simulation of the vehicle–parachute system was conducted. The Moving Computational Domain method employed in this study translates the computational domain together with the object, enabling efficient numerical simulation of large-scale motion without relying on a fixed computational domain [16]. The FSI framework presented in this study will serve as an efficient verification platform for the design optimization and safety assessment of emergency parachutes for flying cars.

2 Numerical Approach

2.1 Governing Equation for the Fluid

To simulate the flow field around the parachute, the three-dimensional Euler equations are employed. Although the actual flow is viscous and at a high Reynolds number, the present study focuses on capturing the global flow structure and enabling coupled simulation with the structural solver. Therefore, viscous terms are neglected, and the governing equations are written in conservative form as follows:

$$\frac{\partial \boldsymbol{q}}{\partial t} + \frac{\partial \boldsymbol{E}}{\partial x} + \frac{\partial \boldsymbol{F}}{\partial y} + \frac{\partial \boldsymbol{G}}{\partial z} = 0 \tag{1}$$

$$\boldsymbol{q} = \begin{pmatrix} \rho \\ \rho u \\ \rho v \\ \rho w \\ e \end{pmatrix}, \boldsymbol{E} = \begin{pmatrix} \rho u \\ \rho u^2 + p \\ \rho uv \\ \rho uw \\ u(e+p) \end{pmatrix}, \boldsymbol{F} = \begin{pmatrix} \rho v \\ \rho uv \\ \rho v^2 + p \\ \rho vw \\ v(e+p) \end{pmatrix}, \boldsymbol{G} = \begin{pmatrix} \rho v \\ \rho uv \\ \rho v^2 + p \\ \rho vw \\ v(e+p) \end{pmatrix} \tag{2}$$

Here, $\boldsymbol{q}$ denotes the vector of conserved variables, and $\boldsymbol{E}, \boldsymbol{F}$, and $\boldsymbol{G}$ are the inviscid flux vectors in the x-, y-, and z-directions, respectively. The unknowns are the density ρ,

ICCS Camera Ready Version 2026
To cite this paper please use the final published version:
DOI: 10.1007/978-3-032-29921-5_7

the velocity components $u, v,$ and w in the x-, y-, and z-directions, and the total energy per unit volume e. The pressure p is given, for a perfect gas, by the following relation.

$$p = (\gamma - 1)\left\{e - \frac{1}{2}\rho(u^2 + v^2 + w^2)\right\} \tag{3}$$

Here, γ is the ratio of specific heats, which is set to 1.4 in this study. In the flow-field simulations, the canopy and the vehicle are treated as solid walls with a slip boundary condition. On the outer boundaries, Riemann boundary conditions are imposed [17].

2.2 Unstructured Moving-Grid Finite-Volume Method

In this study, we simulate the flow field around a deformable parachute undergoing elastic deformation. To compute the flow induced by the motion of the canopy wall, we employ an unstructured moving-grid finite-volume method [10, 11]. To satisfy the geometric conservation law, the numerical fluxes are evaluated over control volumes defined in a unified space–time domain (x, y, z, t). The primary variables are stored and evaluated at cell centers. In addition, the moving computational domain (MCD) method based on this formulation [16] translates the entire computational domain containing the body together with the body itself. This enables the flow field associated with the parachute motion to be computed without being constrained by the domain size. A schematic of the MCD method is shown in Fig. 1.

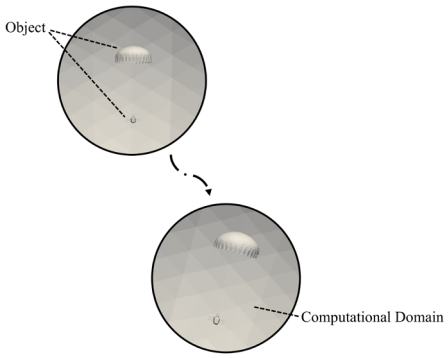

Fig. 1. Schematic of the MCD method

2.3 Spring-Mesh Method

As described above, the wall boundary deforms according to the elastic deformation of the canopy. To preserve the quality of the interior cells of the fluid mesh, we employ a spring-mesh method [18]. In this approach, mesh nodes are assumed to be connected by tensile springs. The spring constants are defined so as to maintain mesh quality (e.g., edge lengths and face angles), and the updated node positions are obtained by solving for the equilibrium configuration in which the forces induced by the springs are balanced. An example of the resulting mesh deformation is shown in Fig. 2.

ICCS Camera Ready Version 2026
To cite this paper please use the final published version:
DOI: 10.1007/978-3-032-29921-5_7

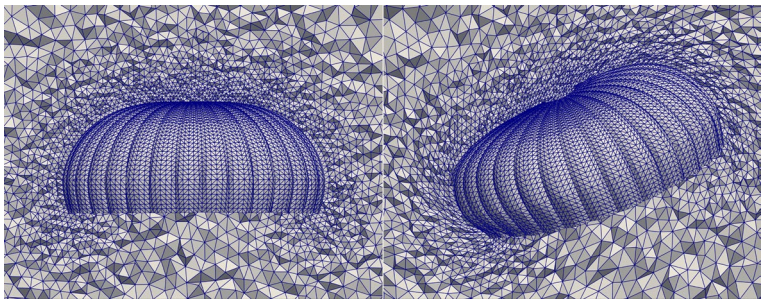

Fig. 2. Unstructured mesh deformation based on the spring-mesh method

2.4 Project Chrono

To model the elastic deformation of the parachute, we use Project Chrono. Project Chrono is an open-source framework for physics-based modeling and simulation, supporting, for example, vehicles, robots, mechatronic systems, and multiphysics problems including fluid–solid interactions [12, 13]. Using this framework, the canopy is modeled with Kirchhoff–Love thin-shell elements based on the BST formulation, the reinforcement cables and suspension lines are modeled with ANCF beam elements (Euler–Bernoulli), and the vehicle is modeled as a rigid body [13]. These modeling choices have also been adopted in previous studies [14, 15] and are suitable for computing large elastic deformations in parachute systems. In the present work, Project Chrono is used to perform structural dynamics simulations in a fully dimensional form.

2.5 Fluid–Structure Coupling Method

In this study, the structural and fluid governing equations are solved sequentially and separately at each time step. The pressure on the canopy surface obtained from the fluid solver is applied to the structural solver as an external load, whereas the canopy surface velocity computed by the structural solver is imposed in the fluid solver as a prescribed velocity boundary condition. Using the structural surface velocity, the boundary mesh is updated, and the interior cells are subsequently smoothed using the spring-mesh method. The flow solution is then advanced on the deformed mesh. Within a single time step, the interface data are exchanged only once in each direction; thus, the framework employs a two-way weakly coupled partitioned scheme. In addition, the shell discretization used in the structural solver and the surface mesh used in the fluid solver are fully conforming, with a one-to-one correspondence of interface nodes.

3 Wind-Tunnel Simulation

3.1 T-10 Type Parachute

We adopt the U.S. Army T-10 parachute [19] as a reference configuration. It is a flat-extended-skirt parachute consisting of a canopy (fabric membrane) and 30 suspension

ICCS Camera Ready Version 2026
To cite this paper please use the final published version:
DOI: 10.1007/978-3-032-29921-5_7

lines. A schematic of the parachute configuration is shown in Fig. 3. In the manufactured (stress-free) configuration, the canopy comprises a flat main circular panel with a circular vent at the apex and a flat skirt section (annular ring) below it, with their outer circumferences joined. The suspension lines are attached to the inner circumference of the skirt, pass through the canopy, extend as gore reinforcement cables, and merge at the apex. Following previous studies [14, 15], the structural diameter D_c is set to 10.67 m and the line length l_e to 8.96 m. The vent diameter D_v and the skirt width are both assumed to be $0.1D_c$. The geometric symbols are defined according to the notation in Refs. [20, 21]. With these parameters, the canopy surface area S_o, including the vent area of 0.894 m^2, is 122 m^2, giving a nominal diameter D_o (based on S_o) of 12.4 m.

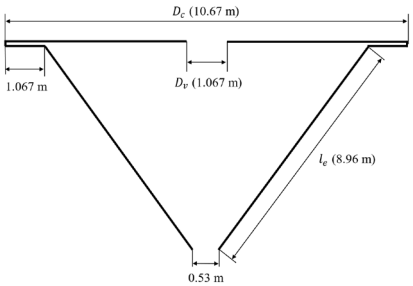

Fig. 3. Schematic of the parachute

3.2 Computational Mesh

Figure 4 shows the computational meshes used in this study: (a) an exploded view of the structural mesh and (b) the fluid mesh. The number of surface mesh elements is 12,870. The fluid mesh is generated using MEGG3D [22, 23]. The reference length L is taken to be equal to D_c (10.67 m), and the diameter of the spherical computational domain is set to $30L$. The resulting fluid mesh contains 840,908 cells. The reference velocity and density are set to 340.29 m/s and 1.247 kg/m^3, respectively.

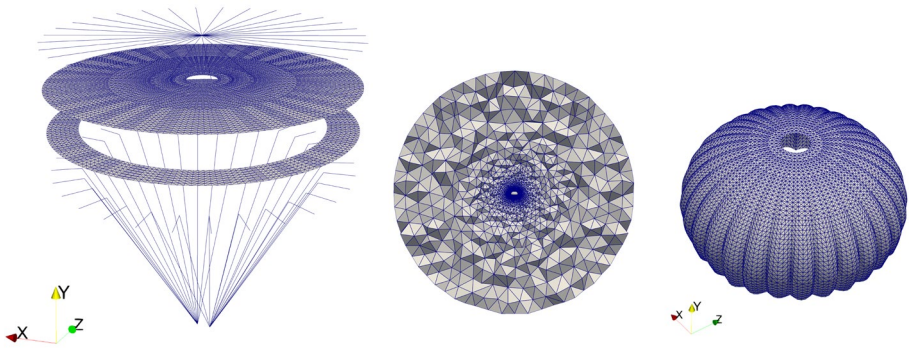

(a) Structural mesh (exploded view) (b) Fluid mesh

Fig. 4. Computational meshes: (a) structural mesh (exploded view) and (b) fluid mesh

ICCS Camera Ready Version 2026
To cite this paper please use the final published version:
DOI: 10.1007/978-3-032-29921-5_7

3.3 Material Properties

The Young's modulus, Poisson's ratio, density, and thickness (or diameter) of the canopy and cables are taken from the validation studies [14, 15], and the corresponding material properties are summarized in Table 1.

Table 1. Material properties of parachute

	Canopy	Suspension line	Radial reinforcement
Elements	12870	12	45
Young's modulus, Pa	9.57×10^{6}	2.07×10^{8}	2.07×10^{8}
Poisson ratio	0.3	—	—
Density, kg/m^3	3090	3090	3090
Thickness (Diameter), m	3.04×10^{-5}	3.43×10^{-3}	3.43×10^{-3}

3.4 Simulation Condition

Simulations are performed under conditions corresponding to the validation cases in Refs. [14, 15], and the results are comparatively assessed. The simulations for Cases 1–3 follow the procedure described below.

1. The ends of the suspension lines are fully constrained at two points in space, and a uniform internal pressure of 23.9 Pa is applied to the canopy to obtain a steady inflated configuration via structural simulation. To suppress canopy oscillations, a damping force proportional to the nodal velocities is added. The distance between the two constrained points at the suspension line ends is set to 0.53 m.
2. Using the steady canopy shape obtained in Case 1 as a fixed wall boundary, a flow simulation is performed with a uniform upward freestream velocity of 6.7 m/s. This condition corresponds to the dynamic pressure of 23.9 Pa applied in Case 1, and the Reynolds number is approximately 5.0×10^{6}.
3. Using the results of Cases 1 and 2 as initial conditions, an FSI simulation is conducted with the same upward freestream velocity of 6.7 m/s, in which the canopy is treated as a deformable boundary. The suspension line ends remain constrained in this case.

Gravity is not included in Cases 1–3. For comparative validation, Cases 1 and 2 are carried out for two parachute configurations: with and without reinforcement cables. In Cases 1 and 2, the nondimensional time step is set to 0.002 (corresponding to a dimensional time step of 6.27×10^{-5} s), whereas in Case 3 the nondimensional time step is set to 0.001 (corresponding to 3.14×10^{-5} s).

3.5 Results

Steady-State Inflated Canopy Shape. Figure 5 shows the steady inflated canopy shapes obtained from Case 1: the left panel corresponds to the case with reinforcement cables and the right panel to the case without reinforcement cables. With reinforcement

ICCS Camera Ready Version 2026
To cite this paper please use the final published version:
DOI: 10.1007/978-3-032-29921-5_7

cables, the projected diameter D_p is 8.63 m. An empirical correlation derived from experiments in Ref. [21] predicts a projected diameter of approximately 8.44 m for a parachute with a structural diameter D_C of 10.67 m, indicating good agreement. In contrast, without reinforcement cables, D_p increases to 9.21 m, indicating a greater inflation level; in terms of projected area, the difference is approximately 19.1%. These results indicate that reinforcement cables suppress canopy inflation due to increased structural stiffness, although the magnitude is expected to depend on the actual stiffness and layout. Because drag varies approximately in proportion to the projected area, the presence or absence of reinforcement cables is likely to significantly affect the parachute's drag performance.

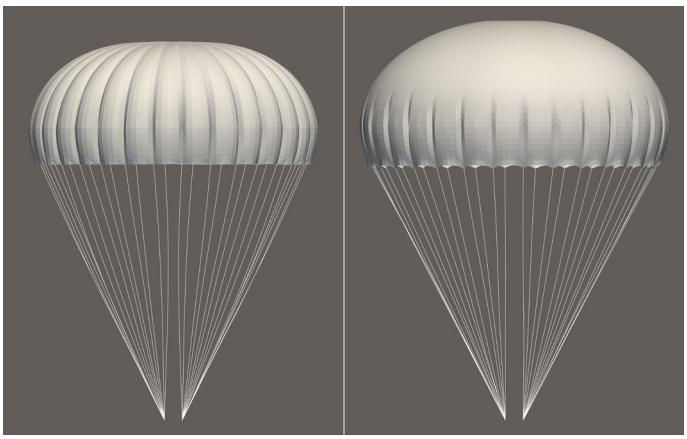

Fig. 5. Steady-state inflated canopy shape (left: with reinforcement cables; right: without reinforcement cables)

Fluid-Only Simulation with Fixed Walls. Figure 6 visualizes the velocity vectors and pressure distribution obtained in Case 2 for the parachute with reinforcement cables. The velocity vectors (left) indicate that the flow separated at the skirt edge forms a large-scale wake vortex, in qualitative agreement with the validation studies [14, 15]. These results indicate that, even with the Euler equations, skirt-edge separation and the resulting global wake vortex can be captured with numerical dissipation acting as an effective trigger. The pressure distribution (right) indicates a low-pressure region extending toward the vortex core. The large drag is primarily generated by the pressure difference between the low pressure in the wake vortex and the positive pressure inside the canopy associated with flow stagnation.

Here, two drag coefficients, C_{D_p} and C_{D_o}, are defined as follows:

$$C_{D_p} = \frac{F_D}{\frac{1}{2}\rho U^2 S_p}, \qquad C_{D_o} = \frac{F_D}{\frac{1}{2}\rho U^2 S_o} \tag{4}$$

Here, F_D denotes the drag force, ρ the density, and U the freestream velocity. The coefficient C_{D_p} is defined using the projected area S_p as the reference area, whereas C_{D_o}

ICCS Camera Ready Version 2026
To cite this paper please use the final published version:
DOI: 10.1007/978-3-032-29921-5_7

is defined using the pre-inflation surface area S_o. Because C_{D_o} does not depend on the instantaneous S_p, its relative variation directly reflects that of F_D, and it is commonly used as an indicator of drag performance per unit canopy surface area.

In the validation cases [14, 15], C_{D_o} is 0.72, whereas the present result for the reinforced parachute is approximately 0.62, which is 86.1% of the reference value. The drag force was obtained by integrating the surface pressure over the canopy. This is because viscous effects are not included in the Euler equations, and pressure drag is dominant for bluff bodies such as parachutes, where flow separation induces a large pressure difference between the front and rear surfaces. However, because boundary-layer development and turbulence effects are not considered in the present simulation, shear-layer diffusion is underestimated. This suppresses wake spreading and results in an artificially narrow wake region. Consequently, the base pressure behind the canopy is overpredicted, leading to a reduced pressure difference and an underestimation of the drag.

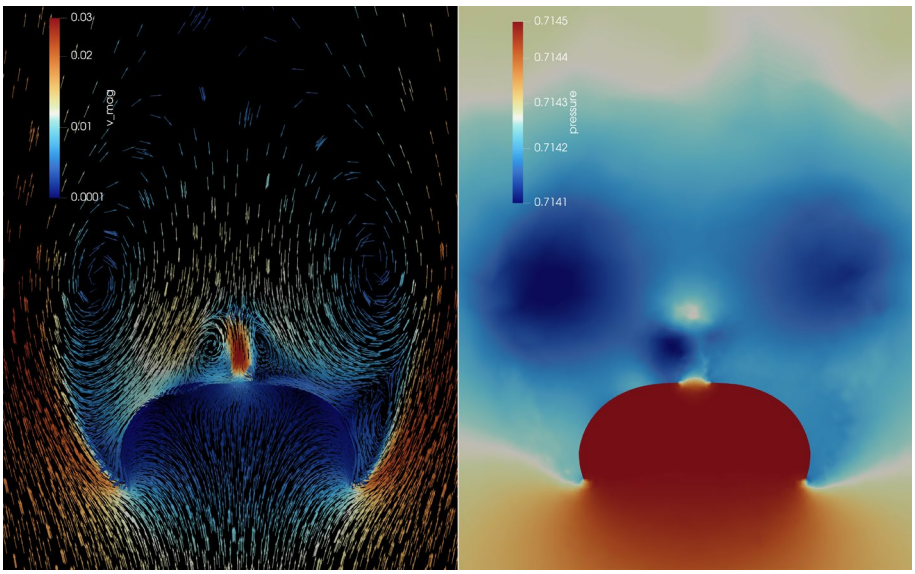

Fig. 6. Flow field around the canopy (left: velocity vector distribution; right: pressure distribution)

FSI Wind-Tunnel Simulation. Figure 7 presents the time histories of the drag coefficient C_{D_o} obtained from Cases 2 and 3 for the rigid and elastic models. In the elastic model, the initial stage of the FSI simulation strongly influences the aerodynamic response. Immediately after the onset of coupling, the internal high pressure within the canopy is relieved due to wall expansion, resulting in a temporary decrease in drag. Subsequently, periodic oscillations appear in the drag coefficient of the elastic model, whereas no such behavior is observed in the rigid model. To investigate the origin of these oscillations, Figure 8 shows the time histories of the projected area S_p and the

ICCS Camera Ready Version 2026
To cite this paper please use the final published version:
DOI: 10.1007/978-3-032-29921-5_7

drag coefficient defined with respect to the projected area, C_{D_p}. The projected area exhibits periodic variations corresponding to repeated inflation and contraction of the canopy, i.e., the breathing motion of parachutes [24]. This breathing motion is driven by periodic vortex structures in the near wake that induce suction on the canopy surface and thus arises from fluid–structure interaction. The phase of the projected-area oscillation does not necessarily coincide with that of the drag fluctuation, and the results indicate that the overall drag variation is primarily governed by oscillations in C_{D_p}. This suggests that drag fluctuations cannot be attributed solely to geometric changes in the projected area. Rather, acceleration associated with canopy deformation induces added-mass-like effects in the surrounding fluid, thereby amplifying the drag through unsteady fluid–structure coupling [24]. These drag oscillations directly affect the descent velocity of the vehicle. The elastic model successfully captures FSI-induced phenomena that cannot be reproduced by the rigid model.

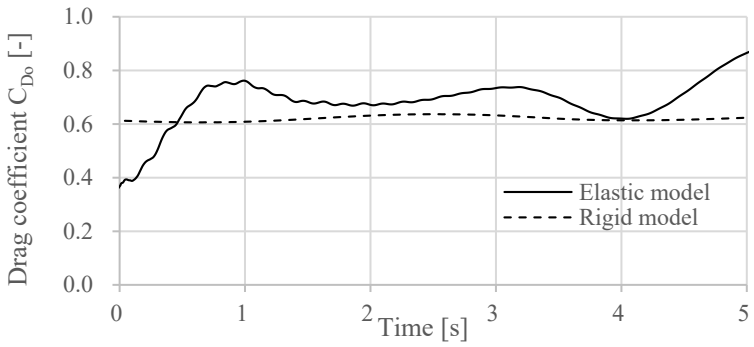

Fig. 7. Time history of drag coefficient C_{D_o} for rigid and elastic models

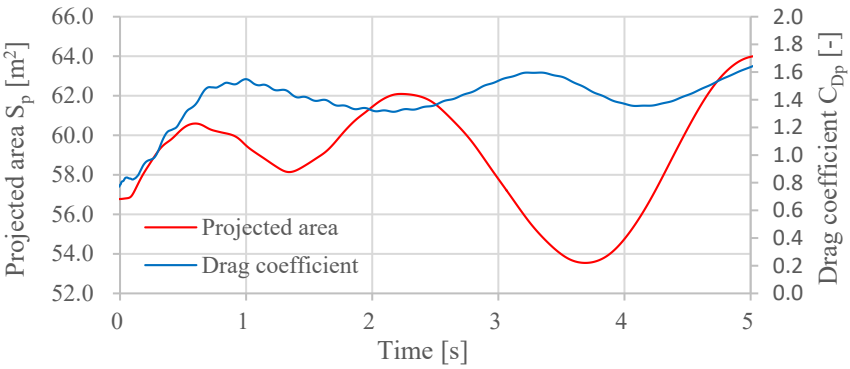

Fig. 8. Time history of projected area S_p and drag coefficient C_{D_p} for elastic model

ICCS Camera Ready Version 2026
To cite this paper please use the final published version:
DOI: 10.1007/978-3-032-29921-5_7

4 Freefalling Parachute System for a Flying Car

4.1 Simulation Conditions for Free Fall

A free-fall simulation was performed for a rigid–elastic system consisting of a parachute connected to a vehicle via suspension lines. The parachute is modeled as an elliptical canopy with a surface area S_o of 110 m^2 and a mass of 9 kg, based on manufacturer specifications [25]. The material properties of the canopy are taken from Ref. [26], and those of the 30 suspension lines are taken from Ref. [27]; these values are summarized in Table 2. The vehicle is modeled after the SD-03 developed by SkyDrive Inc., Japan [28]. The vehicle mass is set to 400 kg, and the principal moments of inertia about the center of gravity (I_{xx}, I_{yy}, I_{zz}) are set to (50.4, 344, 334) kg·m^2. First, under a gravitational acceleration of 9.81 m/s^2, the stress-free rigid–elastic system was allowed to undergo one second of free fall without aerodynamic forces. This procedure resulted in a velocity of 9.81 m/s and simultaneously established a numerically consistent initial flow field, thereby suppressing artificial aerodynamic transients at the onset of the FSI computation. Subsequently, the FSI simulation was initiated from this state, and the free-fall motion, including aerodynamic drag acting on both the canopy and the vehicle, was simulated.

Table 2. Material properties of parachute

	Canopy	Suspension line
Elements	9780	16
Young's modulus, Pa	4.60×10^{8}	2.25×10^{9}
Poisson ratio	0.14	–
Thickness (Diameter), m	1.00×10^{-4}	5.58×10^{-3}

4.2 Computational Mesh

Figure 9 shows the fluid and structural computational meshes generated using MEGG3D [22, 23]. The numbers of surface mesh elements for the canopy and the vehicle are 9,780 and 12,850, respectively. The reference length L is taken to be equal to the vehicle length (4 m), and the diameter of the spherical computational domain is set to $30L$. The resulting fluid mesh consists of 1,239,654 cells. The entire computational domain is translated and rotated according to the motion of the vehicle center of gravity, while the canopy moving wall boundary is deformed in the absolute coordinate system. The reference velocity and density are set to 340.29 m/s and 1.247 kg/m^3, respectively. The nondimensional time step is set to 0.002 (corresponding to a dimensional time step of 2.35×10^{-5} s).

ICCS Camera Ready Version 2026
To cite this paper please use the final published version:
DOI: 10.1007/978-3-032-29921-5_7

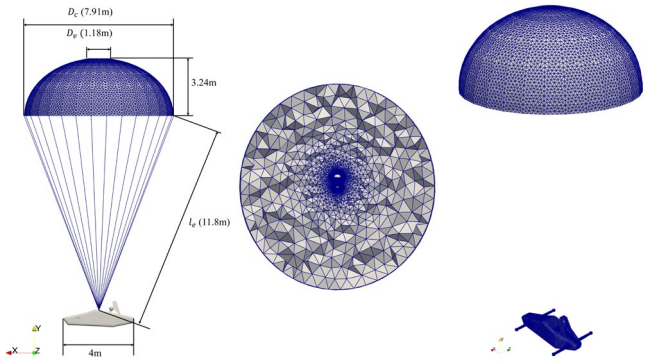

(a) Structural mesh (b) Fluid mesh

Fig. 9. Structural mesh, computational domain, and fluid surface mesh

4.3 Results

Figure 10 shows the total drag acting on the canopy and the vehicle, together with the magnitude of the vehicle's vertical descent velocity. The descent velocity decreases from 9.81 m/s to 8.53 m/s over approximately 1.43 s. During this period, the drag converges to a value nearly equal to the combined weight of the parachute and the vehicle (equivalent to about 4.01 kN), indicating that a steady descent state is reached in which drag and gravity are balanced. Figure 11 visualizes the free-fall behavior of the vehicle–parachute system, showing a contour of the Q-criterion at 0.001. After about 4 s, the vehicle attitude begins to tilt and oscillatory motion develops. As the oscillation angle increases, the drag also increases, indicating that the oscillation tends to be amplified. This behavior suggests static instability of the vehicle–parachute system [21]. Subsequently, periodic oscillatory motion continues within a certain range of oscillation angles. These results demonstrate that the present simulation successfully reproduces the process by which the parachute decelerates the descent of the flying car.

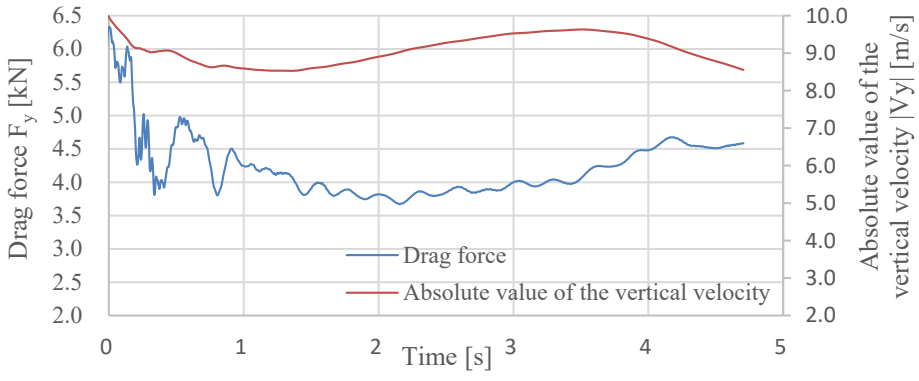

Fig. 10. Time history of drag and vertical velocity

ICCS Camera Ready Version 2026
To cite this paper please use the final published version:
DOI: 10.1007/978-3-032-29921-5_7

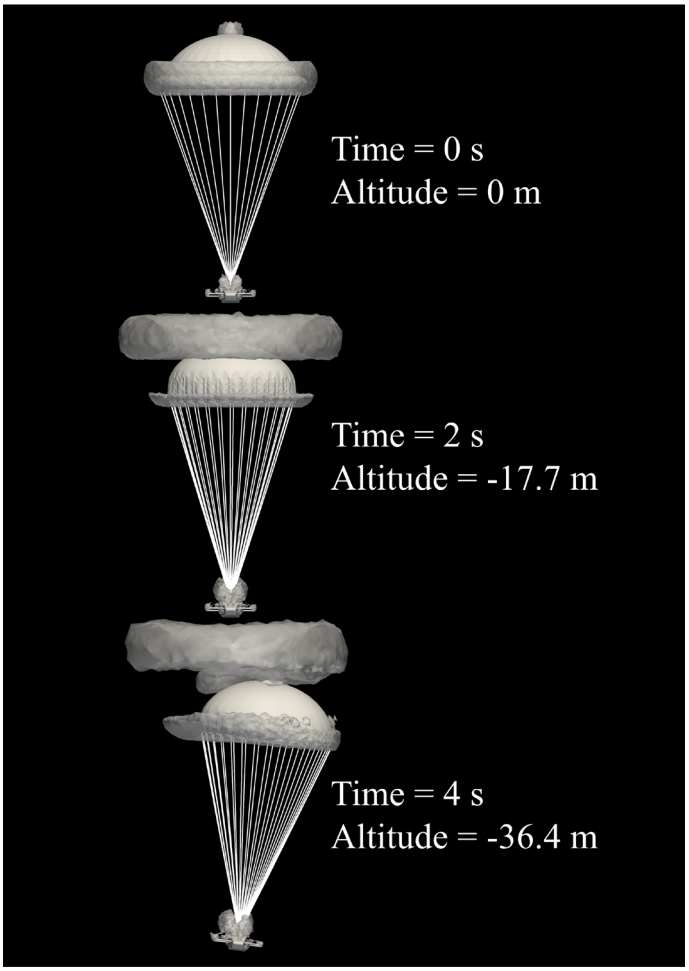

Fig. 11. Free-fall behavior of the vehicle–parachute system with a Q-criterion contour at 0.001

5 Conclusions

In this study, a fluid–structure interaction (FSI) simulation framework was constructed by weakly coupling a moving-boundary fluid solver with a structural solver for an emergency recovery parachute intended for a flying car. The behavior of the vehicle–parachute system was evaluated under both wind-tunnel and free-fall conditions. The results demonstrate that gore reinforcement cables govern the inflated canopy shape and constitute a primary factor in determining the mean drag, while canopy elasticity generates unsteady drag components that do not appear in a rigid model. Furthermore, the free-fall simulation successfully reproduced the deceleration process associated with drag development and the transition to a quasi-steady descent state.

ICCS Camera Ready Version 2026
To cite this paper please use the final published version:
DOI: 10.1007/978-3-032-29921-5_7

On the other hand, discrepancies from reference results were also observed, including an underestimation of the drag coefficient. However, for parachutes, where the flow field is largely insensitive to the Reynolds number [21], the Euler equations can be considered an effective approximation from the viewpoints of computational cost and accuracy, provided that appropriate modeling is employed.

Future work will focus on quantitatively assessing the limitations in reproducing physical phenomena due to the neglect of viscous and turbulent effects. In addition, the robustness of mesh-shape preservation in the moving-grid computation will be improved. Further investigations will be conducted under more realistic operating conditions, including low-altitude deployment, initial vehicle attitude, and wind disturbances. Ultimately, the proposed framework will be extended into a quantitative evaluation methodology applicable to design optimization and safety assessment.

Acknowledgments. This paper is based on results obtained from a project, JPNP14004, subsidized by the New Energy and Industrial Technology Development Organization (NEDO).

References

1. Pan, G., Alouini, M.-S.: Flying Car Transportation System: Advances, Techniques, and Challenges. IEEE Access 9, 24586–24603 (2021)
2. Straubinger, A., Rothfeld, R., Shamiyeh, M., Büchter, K.-D., Kaiser, J., Plötner, K.O.: An overview of current research and developments in urban air mobility – Setting the scene for UAM introduction. Journal of Air Transport Management 87, 101852 (2020)
3. Thompson, E., Taye, A., Guo, W., Wei, P., Quinones-Grueiro, M., Ahmed, I., Biswas, G., Quattrociocchi, J., Carr, S., Topcu, U., Jones, J., Brittain, M.: A Survey of eVTOL Aircraft and AAM Operation Hazards. In: AIAA AVIATION 2022 Forum, p. 3539 (2022)
4. Courtin, C., Hansman, R.J.: Safety Considerations in Emerging Electric Aircraft Architectures. In: 2018 Aviation Technology, Integration, and Operations Conference (ATIO), AIAA Paper 2018-4149 (2018)
5. XPENG AEROHT Innovative Multi-Parachute Safety System. YouTube, https://www.youtube.com/watch?v=Q2Z7urKB0aY, last accessed 2026/02/05
6. BRS Aerospace: Whole Aircraft Recovery Parachute Systems. https://brsaerospace.com/, last accessed 2026/02/05
7. Hinman, B.L.: eVTOLs and Autorotation: Designing for Maximum Safety. Medium, Sep 11, 2019. https://brian-is-flyin.medium.com/evtols-and-autorotation-designing-for-maximum-safety-264a970c9299, last accessed 2026/02/05
8. Mellor, R.: Emergency Descent Arrest Systems (EDAS) for VTOL Aircraft (Draft White Paper). Advanced Blast, Feb 16, 2021. https://www.advanced-blast.com/emergency-descent-arrest-systems-edas-for-vtol-aircraft-draft-white-paper/, last accessed 2026/02/05
9. Takizawa, K., Tezduyar, T.E.: Computational Methods for Parachute Fluid–Structure Interactions. Archives of Computational Methods in Engineering 19, 125–169 (2012)
10. Yamakawa, M., Matusno, K.: Unstructured moving-grid finite-volume method for unsteady shocked flows. J. Comput. Fluids Eng. 10–1,24–30 (2005)
11. Yamakawa, M., Takekawa, D., Matsuno, K., Asao, S.: Numerical simulation for a flow around body ejection using an axisymmetric unstructured moving grid method. Comput. Therm. Sci. 4(3), 217–223 (2012)
12. Project Chrono: Official Website. https://projectchrono.org/, last accessed 2026/02/10

ICCS Camera Ready Version 2026
To cite this paper please use the final published version:
DOI: 10.1007/978-3-032-29921-5_7

13. Tasora, A., Serban, R., Mazhar, H., Pazouki, A., Melanz, D., Fleischmann, J., Taylor, M., Sugiyama, H., Negrut, D.: Chrono: An Open Source Multi-physics Dynamics Engine. In: Kozubek, T. (ed.) High Performance Computing in Science and Engineering, LNCS, pp. 19–49. Springer, Cham (2016)
14. Stein, K., Benney, R., Kalro, V., Tezduyar, T.E., Leonard, J., Accorsi, M.: Parachute Fluid–Structure Interactions: 3-D Computation. Computer Methods in Applied Mechanics and Engineering 190(3–4), 373–386 (2000)
15. Stein, K.R., Benney, R.J., Tezduyar, T.E., Leonard, J.W., Accorsi, M.L.: Fluid-Structure Interactions of a Round Parachute: Modeling and Simulation Techniques. Journal of Aircraft 38(5), 800–808 (2001)
16. Gomi, R., Takii, A., Yamakawa, M., Asao, S., Takeuchi, S., Nishimura, M.: Flight simulation from takeoff to yawing of eVTOL airplane with coaxial propellers by fluid-rigid body interaction. Advances in Aerodynamics 5(1), 2 (2023)
17. Hirsch, C.: Numerical Computation of Internal and External Flows, Vol. 2: Computational Methods for Inviscid and Viscous Flows. Wiley, Chichester (1988)
18. Murayama, M., Nakahashi, K., Matsushima, K.: A Robust Method for Unstructured Volume/Surface Mesh Movement. Transactions of the Japan Society for Aeronautical and Space Sciences 46(152), 104–112 (2003)
19. Mills Manufacturing: T-10 Parachute Assembly (T-10 Series Characteristics). https://www.millsmanufacturing.com/products/t-10-parachute/, last accessed 2026/02/10
20. Ewing, E.G., Bixby, H.W., Knacke, T.W.: Recovery System Design Guide. Air Force Flight Dynamics Laboratory, Air Force Wright Aeronautical Laboratories, Wright-Patterson AFB, OH, Report AFFDL-TR-78-151 (1978)
21. Knacke, T.W.: Parachute Recovery Systems Design Manual. Naval Weapons Center, China Lake, CA, ADA247666 (1991)
22. Ito, Y., Nakahashi, K.: Surface triangulation for polygonal models based on CAD data. Intern. J. Numer. Methods Fluids 39(1), 75–96 (2002)
23. Ito, Y.: Challenges in unstructured mesh generation for practical and efficient computational f luid dynamics simulations. Comput. Fluids 85,47–52 (2013)
24. Johari, H., Desabrais, K.J.: Vortex shedding in the near wake of a parachute canopy. Journal of Fluid Mechanics 536, 185–207 (2005)
25. SkyEagle Parachute: T191 Aircraft Emergency Parachute (Low Altitude Multirotor & eVTOL Solutions). https://www.skyeagleparachute.com/product/t191-aircraft-emergency-parachute-low-altitude-multirotor-evtol-solutions/, last accessed 2026/02/15
26. Niemi, E.E.: An Improved Scaling Law for Determining Stiffness of Flat, Circular Canopies. U.S. Army Natick Research, Development and Engineering Center, Technical Report TR-92/012 (1992)
27. Barry, C.P., Bergeron, K., Stapleton, S.E., Willis, D.J., Noetscher, G., Charrette, C., Sherwood, J.A.: The Investigation of the Mechanical Behavior of a Braided Parachute Suspension Line Using a Mesomechanical Finite Element Model. Textiles 5(2), 10 (2025)
28. SkyDrive Inc.: Official Website. https://en.skydrive2020.com/, last accessed 2026/02/06

ICCS Camera Ready Version 2026
To cite this paper please use the final published version:
DOI: 10.1007/978-3-032-29921-5_7